Empirical Spectral Characteristics of the Medium near Strong-Motion Seismic Stations of Kamchatka

A.A. Gusev[a,c,†], A.A. Skorkina[b,c,✉]

ª Institute of Volcanology and Seismology, Far Eastern Branch of the Russian Academy of Sciences, blv. Piip 9, Petropavlovsk-Kamchatsky, 683006, Russia

ᵇ Institute of Earthquake Prediction Theory and Mathematical Geophysics, Russian Academy of Sciences, ul. Profsoyuznaya 84/32, Moscow, 117997, Russia

ᶜ Geophysical Survey of the Russian Academy of Sciences, Federal Research Center, Kamchatka Branch, blv. Piip 9, Petropavlovsk-Kamchatsky, 683006, Russia

Abstract—Spectral characteristics of the medium around 23 digital strong-motion seismic stations of Kamchatka region have been studied from local earthquake data relative to a reference bedrock station (Petropavlovsk, PET). Spectra are determined by multiband filtering. In each band peak velocity amplitudes, levels of Fourier S-spectra and mean-square coda amplitudes were compared. Average Fourier spectra were obtained from *S*-wave energy using Parseval's equation. The difference in hypocentral distances for pairs of stations was compensated by empirical *S*-wave attenuation functions. Records of more than 300 events were processed, with $M = 5$–6 and hypocentral distances mainly 100–600 km. The spectral ratios estimated by the three methods show behavior diversity. Some non-rock stations show expected spectral characteristics at high frequencies. The conditions at other stations can be considered similar to those at PET. Some stations show amplifications of up to 10 times in the 20–30 Hz frequency range. In general, the obtained spectral characteristics within 3–5 Hz are consistent with the expected trends corresponding to known local geology around strong-motion stations.

Keywords: S-wave, coda, reference station, spectral ratio, site response, strong-motion station, Kamchatka

INTRODUCTION

Investigation into site responses in a frequency range of 0.2 to 30.0 Hz is an indispensable step in seismic risk assessment. A site response is meant as frequency-dependent amplification observed in waves of different periods, which is specific to a construction site or to a site where a seismic station is installed. Such amplification can be estimated using either Fourier or response spectra. The estimates obtained with the Fourier spectra with respect to a reference station we would call "relative response spectrum of the medium" or "empirical spectral characteristics of the medium near seismic stations.

Most of ground studies for seismic risk assessment in Kamchatka have been focused on the area of Petropavlovsk-Kamchatsky city. Systematic work by Shteinberg and Fedotov (1974), as well as Ershov (1974), revealed several ground types with expected strong-motion spectra. Later, specific ground responses were estimated with reference to data from the permanent seismic station of Petropavlovsk (PET) for several sites on contract (Gusev et al., 1980; Gusev, 1990).

The deployment of a digital seismic network in Kamchatka (Chebrov et al., 2013) has made it possible to study site responses systematically in a large range of frequencies (0.2–30.0 Hz) and to cover some sites outside Petropavlovsk-Kamchatsky. These observations provide data for seismic risk assessment in different areas throughout Kamchatka.

Small-scale seismic risk zoning has been conventionally performed by computing Fourier and response spectra (Medvedev, 1977). A response spectrum is a series of peak amplitudes for a set of pendulums with the same attenuation (Q) and different natural frequencies. In fact, the pendulums of this kind make up a multiband filter with a fixed relative bandwidth. Soviet seismologists had a large experience with such filtering technique (Rautian et al., 1981) implemented in frequency-selective seismic stations (Zapolsky, 1971). In this study, a similar approach is applied to digital recordings.

Both approaches in engineering seismology use analysis of *P*- and *S*-wave accelerograms. However, shear waves pay major or predominant contribution to the energy and peak amplitudes of waves, and to displacement (which is especially important in engineering applications), at short distances (Fedotov, 1972). Therefore, shear waves are used as the main analyzed signal in this study.

[†] Deceased.
[✉] Corresponding author.
   E-mail address: anna@mitp.ru (A.A. Skorkina)

Although shear waves are the key component in seismic risk assessment, site amplification can be also studied using *S*-wave coda. As it was found out previously (Phillips and Aki, 1986; Hua et al., 1993), spectral ratios of coda amplitudes are applicable to obtain approximate site responses. The amplitudes are measured as normalized coda spectra: a set of actual mean-square coda amplitudes normalized to a fixed lapse time after the origin time. The analogy of site responses derived from coda and shear waves is physically grounded because coda mainly consists of scattered shear waves, with some contribution of high-frequency surface waves below 2 Hz (Rautian et al., 1981), which also may appear in *S*-waves. Yet, corrections obtained using coda and *S*-wave methods are often poorly consistent (Margheriti et al., 1994; Bonilla et al., 1997). This problem requires special investigation for the conditions of Kamchatka. We present relative response spectra of the medium estimated using Fourier spectra, normalized coda spectra, and analog of spectra recorded at frequency-selective stations which we call "peak amplitude spectra".

Theoretical predictions, e.g., using a layered-earth model (Ratnikova, 1973; Joyner and Fumal, 1984), is an alternative to empirical relative response spectra of the medium. Modeling is possible for 2D and 3D cases, but it requires reliable input data for such calculations, which are not always available.

Modeling is critical for predicting strong ground motion, where nonlinear behavior of grounds is important (Hudson, 1972; Pavlenko and Irikura, 2006). We investigate the ground properties only in the linear approximation (for weak motions), within magnitudes limited to $M = 5$–6.

The consideration below concerns the choice of digital accelerograms of Kamchatka earthquakes; calculations of *S*-wave Fourier, coda, and peak amplitude spectra; calculations of spectral ratios for target and reference sites, as well as analysis of average spectral ratios.

INPUT DATA

Spectral characteristics of the media were studied in Kamchatka were studied from data on 335 events with $M_L = 4.7$–6.4 ($M_w = 4.3$–6.0; $K_S = 11$–14.3) events that occurred at origin depths above 400 km in 2011–2016 (Abubakirov et al., 2018), including the $M_w = 7.2$ Zhupanovskoe earthquake of 30.01.2016 (Chebrov et al., 2016). Altogether we used 7000 records at 23 strong-motion seismic stations (Table 1; Fig. 1); the selected range of magnitudes provided a sufficient signal-to-noise ratio till long distances (Fig. 1*d*).
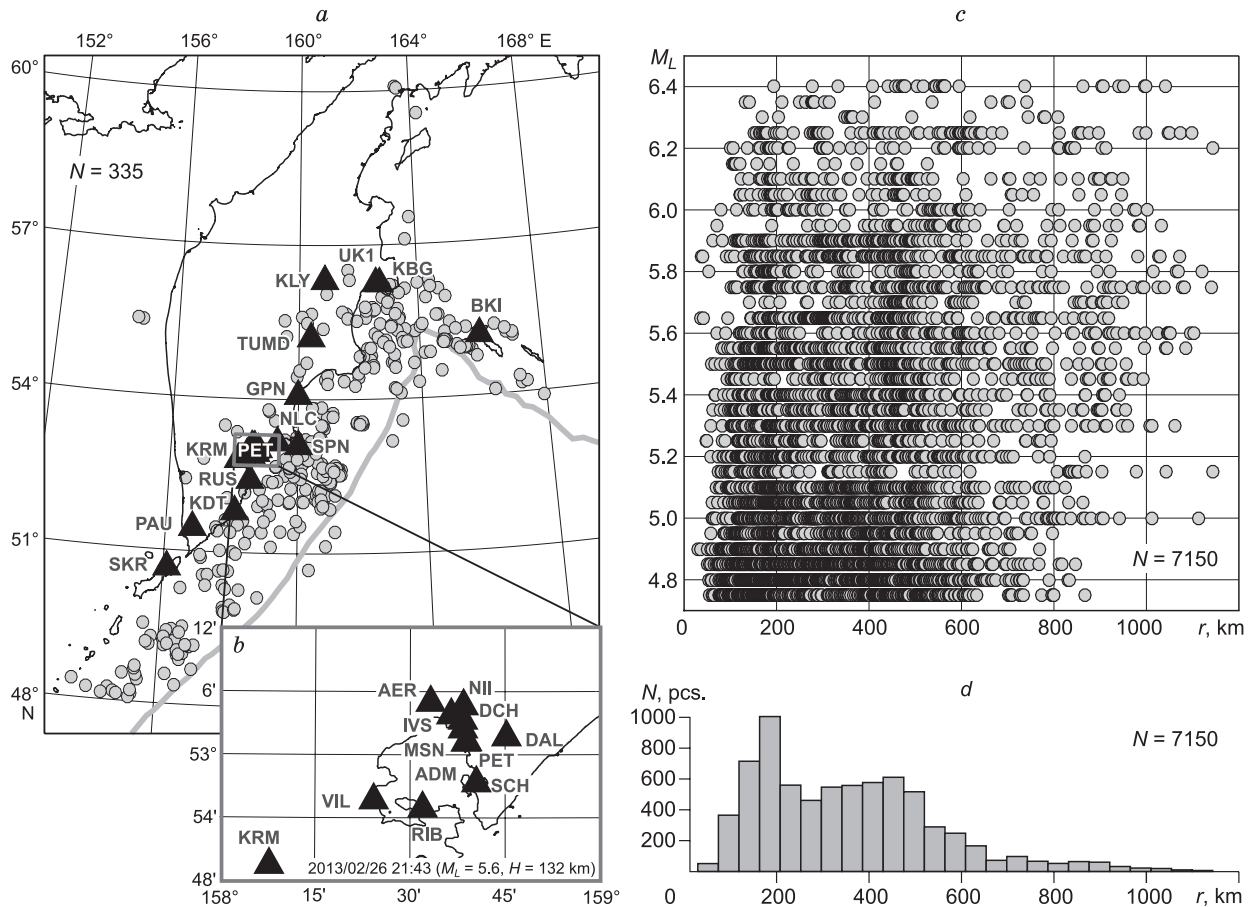
Fig. 1. Data (335 $M_L = 4.7$–6.4 earthquakes for 2011–2016). *a*, Location of seismic stations and earthquakes; *b*, seismic stations of Petropavlovsk cluster (Table 1); *c*, distance (*r*, km) vs. magnitude (M_L) diagram; *d*, distribution of records according to distance.

Table 1. Summary of station sites and grounds

Station/Distance to Δ_{PET}	φ, °	λ, °	h, m	N	Grounds (http://emsd.ru/133-sd)	Local geology
PET Petropavlovsk	53.02	158.65	68	335	Gabbro-dolerite	Large (up to 1 km) gabbro-dolerite intrusion in Cretaceous basement
Stations of Petropavlovsk cluster						
ADM City administration/0.2 km	53.02	158.65	5	306	Soft ground, silt pebble fill	Cretaceous basement covered with thin colluvium
MSN Mishennaya/2.4 km	53.04	158.64	381	238	Hard rock	Rocky eluvium upon Quaternary andesite and dacite lavas
DCH Dachnaya/3.9 km	53.06	158.64	160	317	Average pyroclastics	Volcanic-sedimentary deposits
IVS Institute/5.5 km	53.07	158.61	160	321	Average pyroclastics	Volcanic-sedimentary deposits
NII NIGTC/6.4 km	53.08	158.64	190	282	Consolidated sediments (blocks, debris, clay)	Volcanic-sedimentary deposits
DAL Dalniy/7.0 km	53.03	158.75	57	309	Consolidated sediments (debris, hard rocks)	Cretaceous basement covered with thin colluvium
SCH School/7.4 km	52.96	158.67	70	310	Consolidated sediments (blocks, debris, clay)	Cretaceous basement covered with thin colluvium
AER Aerogeological station/9.5 km	53.09	158.55	80	203	Average ground	Volcanic-sedimentary deposits
RIB Rybachiy/14 km	52.92	158.53	100	320	Consolidated sediments (blocks, debris, clay)	Cretaceous or Paleogene basement covered with thin colluvium
VIL Viluchinsk/19 km	52.93	158.40	40	320	Consolidated sediments (blocks, debris, clay)	Cretaceous or Paleogene basement covered with thin colluvium
KRM Karymshina/41 km	52.83	158.13	100	308	Consolidated sediments (blocks, debris, clay)	Cretaceous or Paleogene basement covered with thin coarse alluvium
Northern stations						
NLC Nalychevo/49 km	53.17	159.35	6	296	–	Cretaceous or Paleogene basement covered with thin colluvium
SPN Shipunskiy/91 km	53.11	160.01	95	282	Hard rock	Cretaceous or Paleogene basement covered with thin colluvium
GPN Zhupanovo/147 km	54.08	159.99	20	247	Hard rock	Volcanic-sedimentary deposits
TUMD Tumrok Springs/268 km	55.20	160.40	478	268	–	Volcanic-sedimentary deposits
KLY Kluchi/393 km	56.32	160.86	35	323	–	Volcanic-sedimentary deposits
UK1 UK administration/440 km	56.26	162.59	5	305	Sand	Poorly consolidated alluvial pebble
KBG Krutoberegovo/445 km	56.26	162.71	30	317	Sand, gravel	Poorly consolidated alluvial pebble
BKI Bering/535 km	55.19	165.98	12	339	Sand, gravel	Conglomerates, medium-size clastic tuff
Southern stations						
RUS Russkaya/66 km	52.43	158.51	125	295	–	Intrusive complex covered with thin colluvium
KDT Khodutka/140 km	51.81	158.08	22	261	Hard rock, lava flow	Cretaceous–Paleogene basement covered with thin colluvium
PAU Pauzhetka/283 km	51.47	156.82	130	313	Sand, gravel	Volcanic-sedimentary deposits
SKR Severo-Kurilsk/321 km	50.67	156.12	30	337	Sand, gravel	Volcanic-sedimentary deposits

Each station is equipped with CMG5T and CMG5TD broadband digital accelerometers which acquire data at a rate of 100 samples/s (Chebrov et al., 2013). Details of grounds at the station sites are available at the website of the Kamchatka Branch of the Geophysical Survey (http://emsd.ru/133-sd, last visited on 19.11.2018).

Local geology of Petropavlovsk-Kamchatsky city. In terms of local geology (Table 1; Fig. 1*b*), the area of Petropavlovsk-Kamchatsky city belongs to the Petropavlovsk horst composed of folded Upper Cretaceous and Paleogene metamorphic rocks covered with Quaternary sediments consolidated to different degrees varying geographically (Sinelnikova, 1986; Markovskii, 2000). The Late Cretaceous greenstone-facies basement is the oldest in the area. The metasedimentary rocks are intruded by gabbro dolerite, basaltic andesite, and diorite. The reference station (PET) is sited on hard igneous rocks of a gabbro-dolerite intrusion. Cretaceous sediments are often overlain by up to 500 m thick poorly consolidated volcanic sand, ash, and tuff. In the vicinity of Petropavlovsk, these young volcanic-sedimentary rocks appear at the foot of Avachinsky and Koryaksky Volcanoes. They are their responses to seismic effects that control ground motion in the city area. Volcanic-sedimentary rocks show weakly pronounced resonance and broadband amplification effects. Seismic velocities are higher in shallow intrusions.

Local geology of Northern Kamchatka. Northern Kamchatka (Table 1) is mainly a mountainous territory consisting of Cretaceous-Paleogene gabbro, ultramafic rocks, silicic volcanics, and volcaniclastics (Sladnev, 2007) and late Pliocene–early Quaternary sediments that fill depressions. Seismic tomography data from the area (Gorbatov et al., 1999) reveal low-velocity zones at depths to 30 km (occasionally as deep as 150 km), which fall within fields of active volcanism, and high-velocity zones, especially in the Commander Islands (BKI station). This area stands out against the remainder peninsula territory in lower velocity ratios of $v_P/v_S = 1.71$ against 1.73 (Kuzin, 1974) and a thin crust of ~25 km. The Commander Islands are composed of Paleogene and Neogene sediments, tuff, and lavas, about 5 km of total thickness. The BKI station is sited on conglomerates and medium-size tuff (Sidorenko, 1964).

Local geology of Southern Kamchatka. Southern Kamchatka (Table 1) is the southern end of a horst anticlinal structure of betwixt mountains (Sredinnyi Massif) where the crystalline rocks of the uplift join a Late Cretaceous sedimentary basin (Vereshchagin, 1956). The area is free from seismic anomalies (Gorbatov et al., 1999): seismic velocities generally correspond to average values over the Kamchatka Peninsula.

METHODS

Wave spectra. At the first step, *S*-wave spectra are determined for fragments of group *S*-wave records, with estimation of amplitude and frequency-dependent signal-to-noise (S/N) ratios (Skorkina and Gusev, 2017); noisy data of S/N < 3 are rejected. Then spectral analysis is performed for each frequency band of the bandpassed signals at an approximately logarithmic interval of central frequencies: 24 bands, 1/3 octave each (0.1 $\log_{10}$ unit), spaced at 0.1 along the log frequency axis.

The amplitude spectra are determined in filtered data for each band, with

– mean-square noise amplitude in a 60 s window prior to *P* arrival;

– square velocity integral over the *S*-wave window (*ES* hereafter);

– *S*-wave peak amplitude (*AS* hereafter);

– mean-square coda amplitude normalized to 100 s lapse time (*CS* hereafter), in a window varying from band to band (see below).

The *ES* value is used to estimate square amplitude spectra within a bandpass. For the specific case of Parceval's theorem (Jenkins and Watts, 1968), the mean-square signal (mean signal energy) can be expanded into a harmonic series. Thus, the time integral of the current square *S* velocity for each band is converted to a frequency integral of the square amplitude spectrum. The procedure yields central frequencies of the multiband filter; their interpolation is equivalent to a smoothed amplitude spectrum.

A previous study (Gusev and Guseva, 2014) showed that the choice of an individual window for *S* waves in each record is not advantageous much over automatic choice by a certain algorithm. In the conditions of Kamchatka, the length of an *S* wave train is proportional to traveltime due to scattering effects (Petukhin and Gusev, 2003). Note that this approach is valid only for small and medium earthquakes (analyzed in this study), whereas the wave-train length for events larger than $M = 6.5–7.0$ comprises effects of source duration. Therefore, *ES* were estimated by integration over a window of (1.0–1.8) t_S, where t_S is the *S*-wave traveltime.

Distance-dependent attenuation. Commonly, local-scale seismic risk zoning is performed for closely spaced target and reference stations recording distant earthquakes. This approach may pose problems with scarce seismological networks in areas of high seismicity, such as the Kamchatka Peninsula (Table 1; Fig. 1*a*). The distance difference for a pair of stations can be compensated using the attenuation function. Such empirical functions were plotted for Fourier amplitude spectra in each band (Gusev et al., 2017).

The attenuation functions for peak amplitudes are calibration curves like those used for the classical magnitude scales. To obtain empirical attenuation functions, *S*-wave peaks and spectra were normalized to the level of mean-square coda amplitudes in the same record, at a fixed lapse time after the origin time (100 s in this study, with the level A_{s100}), as in (Aki and Chouet, 1975; Rautian and Khalturin, 1978). It is often hard to sample this level with a 100 s lapse time but may be possible at a different lapse time; the respective estimate is then converted to that for 100 s using
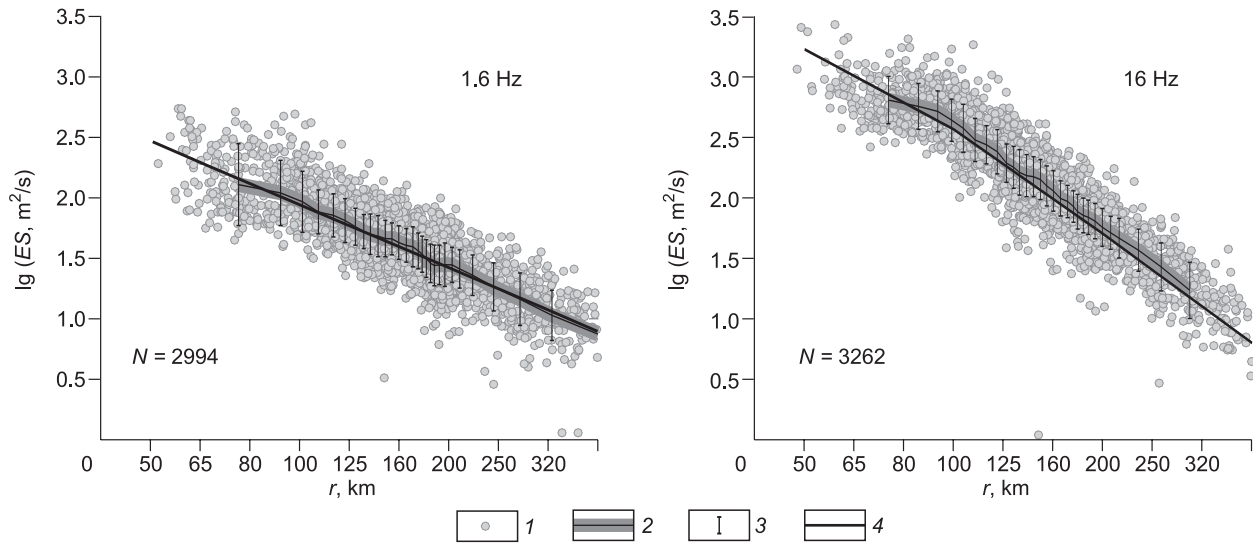
Fig. 2. Energy of shear waves normalized to coda level as a function of distance (*1*), its smoothed version (*2*), standard deviation (*3*), and calibration function (*4*) for *S* waves at 1.6 Hz and 16 Hz.

average regional coda envelopes. The window for coda amplitude estimation is at least $[t_1 - t_2] = 6$ s long, where $t_1 = L_1 t_S$, with L_1 depending on frequency ($L_1 = 2.3$ for 0.25 Hz and $L_1 = 1.7$ for 40 Hz); t_2 depends on noise. The window may be shorter in the presence of aftershocks detected by the automatic algorithm. The attenuation function is found by smoothing the coda-normalized *S*-wave spectral levels (Figs. 2, 3).

The obtained attenuation functions were used to normalize all spectra and amplitudes to a fixed distance of $r_{bas} = 50$ km:

$$S_{ijk,50} = (B_{Sk}(50)/B_{Sk}(r_{ij}))\,S_{ijk}(r_{ij}),$$

$$A_{ijk,50} = (B_{Ak}(50)/B_{Ak}(r_{ij}))\,A_{ijk}(r_{ij}),$$

where S_{ijk} is the Fourier spectra level in a band with the central frequency f_k recorded at the *j*th station during the *i*th earthquake, r_{ij} is the distance of the *j*th station to the *i*th earthquake; $B_{Sk}(r)$ is the normalized attenuation function of the Fourier spectrum for the *k*th band; $S_{ijk,50}$ is the normalized spectrum. Similar equations for peak amplitudes obviously have *A* instead of *S*. Further, only normalized spectra and amplitudes were used. Dividing the normalized spectrum for the station *p* by the respective spectrum for the reference station (number 0), for the same event, gives

$$S_{ipk,50}/S_{i0k,50} = (B_{Sk}(r_{i0})/B_{Sk}(r_{ip}))\,(S_{ipk}(r_{ip})/S_{i0k}(r_{i0})),$$

where the right factor is the ratio of actual spectra and the left one is the distance correction (zero for the reference station). The same notations are valid for peak amplitudes. The recovered coda levels need no normalization.

To study site responses, the logarithms of the calculated spectra

$$\Delta\lg S_{ipk} = \lg(S_{ipk,50}/S_{i0k,50})$$

were averaged:

$$\Delta\lg S_{pk} = (1/n_{pk})\,\Sigma_i\,\Delta\lg S_{ipk},$$

where n_{pk} is the number of recordings. In our case, medians were used instead of mean values, as they are less sensitive to occasional spikes. The variance of $\Delta\lg S_{ipk}$ was characterized by the standard deviation $\sigma(\Delta\lg S_{ipk})$ estimated by a robust algorithm uisng the interquartile range. In the same way,

$$\Delta\lg A_{pk} = (1/n_{pk})\,\Sigma_i\,\lg(S_{ipk,50}/S_{i0k,50}),$$

$$\Delta\lg C_{pk} = (1/n_{pk})\,\Sigma_i\,\lg(A_{c100,ipk}/A_{c100,i0k}).$$

The functions of *S*-wave attenuation and energy and the coda decay functions were plotted by summation of three components. The Fourier and coda spectra were analyzed for mean-square values over horizontal components. The peak amplitudes and mean values were analyzed along the largest horizontal component.

RESULTS

The site responses from records of strong-motion stations operated by the Kamchatka Branch of the Geophysical Survey (Fig. 4) look like smooth curves but they are not actually. The bands do not overlap and the neighbor points are independent, while amplitudes change smoothly in typical cases at the chosen resolution (0.1 stepsize along the log frequency axis). The resolution is illustrated by a few examples of stepwise behavior (KRM, MSN) and spikes, apparently due to resonance (NLC, DAL). The results provide important reference for practical applications, e.g., for seismic risk zoning over Kamchatka or for site corrections in magnitude estimation, etc.
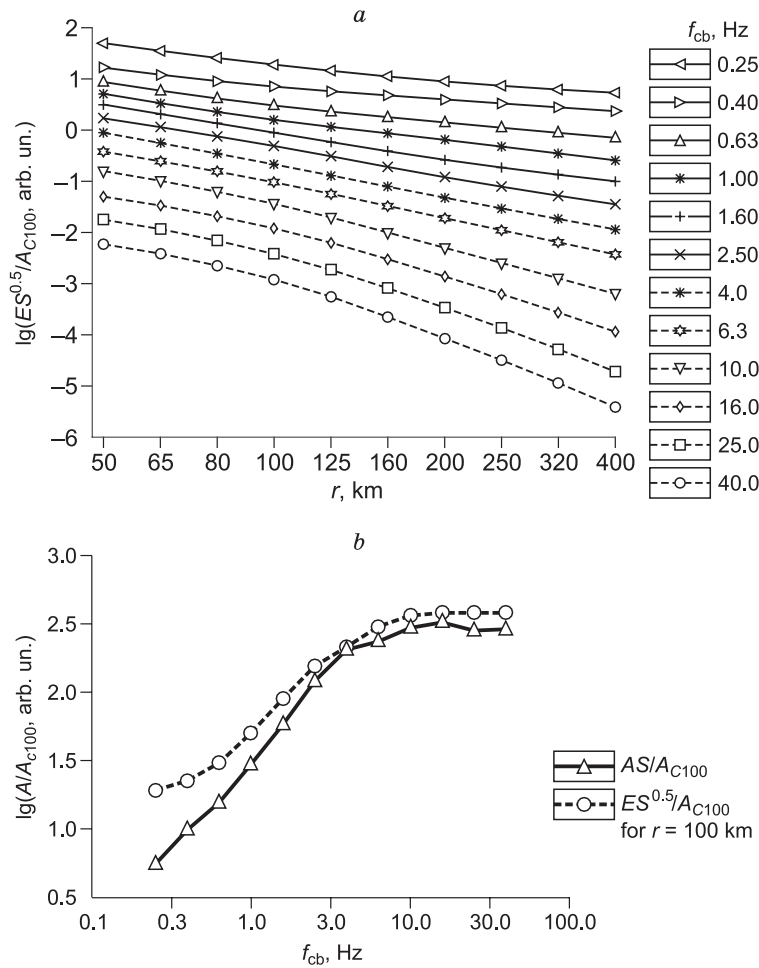
Fig. 3. Examples of attenuation functions. *a*, Attenuation of coda-normalized $(ES)^{0.5}$, i.e., energy of S waves$^{0.5}$, for a thinned set of bands; curves are vertically shifted randomly for better presentation; r is distance (km); f_{cb} is central band frequency; *b*, level tying for curves from panel *a*, at $r = 100$ s; zero ordinate corresponds to $A_i = A_{c\,100}$.

The ground behavior at the sites relative to that at the PET reference station is as follows.

1. The site responses from the ADM and DAL stations are similar to those at the PET station below 1 Hz. Therefore, the subsurface structure beneath these stations differs only within the uppermost 1.2 km, assuming average v_S of 1.2 km/s (Sinelnikova, 1986), but is similar below. The stations are sited on Cretaceous bedrock, which agrees with the State Geological Map (Markovskii, 2000).

2. The responses from DCH, IVS, NII and AER show similar amplification in the 0.3–1.0 Hz range, which may represent a layer of lower density, at least 1.2–4.0 km thick (assuming $v_S = 1.2$ km/s). This pattern likewise agrees with the State Geological Map (Markovskii, 2000): the Nikolsk Fm. crops out at none of these sites.

3. The records at the RUS station show anomalous spectral ratios >1 at 0.2–0.5 Hz, which mean larger amplitudes at the reference station and confirm the presence of a high-velocity layer (higher than beneath PET), at least 2.4–6.0 km thick (assuming $v_S = 1.2$ km/s) corresponding to a large

granite, granodiorite, and alaskite intrusion of the Akhomen complex (Markovskii, 2000). Similar but less pronounced responses in the same band (at 0.2–0.5 Hz) appear at NLC and KRM.

4. The data from southern sites (RUS, KDT, PAU, and SKR) show spectral ratios increasing steadily with frequency above 1 Hz.

5. The responses of northern sites (TUMD, KLY, UK1, KBG, and to a lesser degree GPN) show a distinct decrease in spectral ratios within 1–10 Hz and make up a separate group.

The estimates by different methods (*AS*, *ES*, *CS*) for the same stations agree at some frequencies but more often show different amplifications: the highest for the coda spectra, intermediate for the S-wave Fourier spectra, and the lowest for peak amplitudes. The same distribution can be expected for response spectra. Note that the very presence or absence of difference in the estimates by the three spectral-ratio techniques (*AS*, *ES*, *CS*) correlates with the available knowledge of local geology. The difference is vanishing for
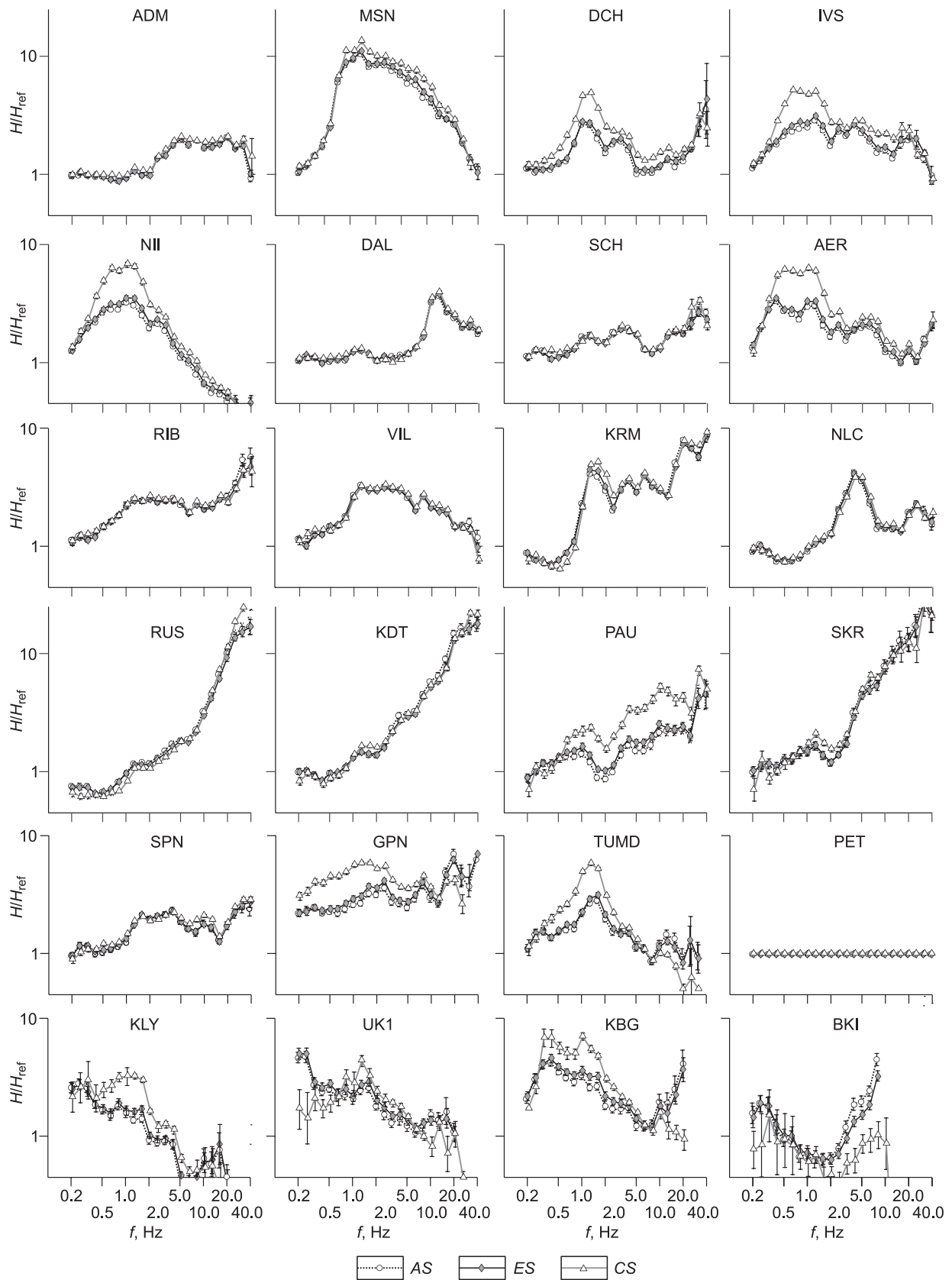
Fig. 4. Site responses recorded at strong-motion stations relative to reference PET station on hard rock. *AS* is peak amplitude spectral ratio, *ES* is *S*-wave Fourier spectral ratio, *CS* is coda spectral ratio. Confidence intervals correspond to conventional standard deviation.

hard rock sites (ADM, DAL, KDT, KRM, NLC, RIB, RUS, SCH, SKR, SPN, and VIL) but is significant for sites on volcanics (IVS, DCH, NII, KLY, and KBG).

Thus, the near-surface structure beneath the ADM, SKR, and NII stations remains poorly resolved (Table 1) and the revealed site responses (Fig. 4) have to be correlated with other data (e.g., drilling). Other features of site responses are interpreted below.

DISCUSSION

The central part of Petropavlovsk-Kamchatsky city was previously divided into six (Shteinberg and Fedotov, 1974) to nine (Ershov, 1974) engineering geological zones. The larger number of zones in the latter case was due to additional measurements at predominant periods, which revealed bedrock outcrops at the SCH site (Ershov, 1974) and has been confirmed by this study. Other site responses from records of PET, ADM, MSN, and DCH accelerometers distributed according to the map of Ershov (1974) roughly agree with rock complexes revealed earlier. The PET and DCH site responses correspond, respectively, to the expected patterns of type 1 (monolith or slightly fractured rocks) and 5 (unconsolidated pyroclastics).

Some observed spectral characteristics may be interpreted differently (Kotha et al., 2016; Alcik, 2018) and thus require additional checks against well-log or core data. For instance, the 1–100 Hz responses of sites in Italy and Turkey reported by Kotha et al. (2016) correlate with average S velocities in the upper 30 m ($v_S 30$) over the rest of the Europe–Middle East region. Since no systematic data on the velocity structure beneath the seismic stations of Kamchatka are available, the interpretation of the obtained site responses can be only preliminary.

1. The amplification in a large band within 10 Hz recorded at MSN may be due to the effect of low impedance, as well as to the effect of topography (Geli et al., 1988): the site is located at the top of a hill with a relative elevation of 350 m (Table 1). The low impedance hardly can be the only cause of amplification: MSN and AER have the same value according to (Shevchenko and Yakovenko, 2018) but the site responses from the two stations are different (Fig. 4).

2. The TUMD and KLY site responses would be attributed to the effect of proximal volcanoes (Kluchevskoy and Kizimen) were they not similar to those of KBG and UK1 located far away on the coast. Another possible cause is that the average attenuation functions like those of Fig. 3 might be poorly applicable to these sites, but the attenuation uncertainty does not influence CS results which generally agree with the ES-based estimates. Anyway, the preliminary results have to be checked.

3. The spectral characteristics obtained for BKI are even more raw, since they show anomalous coda envelope shapes (Lemzikov and Gusev, 1989) besides the doubts in attenuation function applicability. The responses with such coda

envelope shapes would mean greater corrections for coda than for direct S-waves, but the situation is actually inverse.

4. The estimates based on different methods (ES, AS and CS) are markedly dissimilar within certain bands (mainly 0.5–2.0 Hz) for some stations (IVS, DCH, AER, NII, PAU, GPN, TUMD, KLU, and KBG). They are up to twice greater for coda (CS) than for direct S waves (ES, AS), in the bands of highest amplification. The coda amplitudes (i.e., scattered waves) may be greater than expected as a result of superposed slow surface waves (Rautian et al., 1981) that arise in layered basin sediments, but there are no such basins in East Kamchatka. On the other hand, the dissimilarity may be a signature of nonlinear behavior of grounds (Hudson, 1972; Pavlenko and Irikura, 2006), which has to be taken into account in local-scale seismic risk zoning and means that the use of coda amplitudes alone is unacceptable in such areas. In some cases, site effects are estimated using the microtremor technique (Abudeif et al., 2019). However, this method of seismic risk zoning likewise may yield ambiguous results because coda and microtremor signals are of similar nature.

5. The responses of southern sites (RUS, KDT, PAU, and SKR) with spectral ratios increasing with frequency above 1 Hz have never been reported before from Kamchatka. They may represent either some grounds markedly different from those at the reference PET site or strong attenuation at high frequencies beneath PET, which requires further checks.

CONCLUSIONS

1. The suggested and tested multiband method for estimating site effects in spectral responses of grounds implies the use of S-wave peak amplitudes and Fourier spectra, as well as mean-square coda amplitudes. The method allows using records from target and reference stations located at markedly different distances from earthquakes due to empirical regional attenuation functions.

2. The method has been implemented in an automatic mode and tested on hundreds of $M = 5–6$ earthquakes in Kamchatka. Distortions produced by aftershocks superimposed on coda records are removed automatically during amplitude sampling.

3. The collected empirical spectral characteristics of the medium near seismic stations are diverse over a large frequency range of 0.2 to 30.0 Hz and some show resonance amplification effects.

4. The empirical spectral characteristics of the medium near seismic stations obtained in different ways agree qualitatively though there is systematic quantitative difference. Amplification effects are the highest in the coda spectra, intermediate in the S-wave Fourier spectra, and the lowest in the spectra of peak amplitudes. The CS estimates are most often the upper bound for those from S waves, though the amplitudes may be sometimes overestimated (10–20% or

occasionally 100%). The use of coda or microtremor records for seismic risk zoning in Kamchatka may lead to notable errors unless reference to *S*-wave data is made.

REFERENCES

Abubakirov, I.R., Gusev, A.A., Guseva, E.M., Pavlov, V.M., Skorkina, A.A., 2018. Mass determination of moment magnitudes M_w and establishing the relationship between M_w and M_L for moderate and small Kamchatka earthquakes. Izvestiya, Phys. Solid Earth 54, 33–47.

Abudeif, A.M., Fat-Helbary, R.E., Mohammed, M.A., El-Khashab, H.M., Masoud, M.M., 2019. Estimation of the site effect using microtremor technique at new Akhmim city, Akhmim, Sohag, Egypt. Russian Geology and Geophysics (Geologiya i Geofizika) 60 (2), (231–239) (273–282).

Aki, K., Chouet, B., 1975. Origin of coda waves: Source, attenuation, and scattering effects. J. Geophys. Res. 80 (23), 3322–3342.

Alcik, H., 2018. Investigation of local site responses at the Bodrum Peninsula (Southwest of Turkey) using the mainshock and aftershocks of the 20 July 2017 M_w6.6 Bodrum-Kos earthquake. Ann. Geophys. 61 (3), SE339.

Bonilla, L.F., Steidl, J.H., Lindley, G.T., Tumarkin, A.G., Archuleta, R.J., 1997. Site amplification in the San Fernando Valley, California: Variability of site-effect estimation using the S-wave, coda, and H/V methods. Bull. Seismol. Soc. Am. 87 (3), 710–730.

Chebrov, V.N., Droznin, D.V., Kugaenko, Yu.A., Levina, V.I., Senyukov, S.L., Sergeev, V.A., Shevchenko, Yu.V., Yashchuk, V.V., 2013. The system of detailed seismological observations in Kamchatka in 2011. J. Volcanol. Seismol. No. 1, 16–36.

Chebrov, V.N., Kugaenko, Iu.A., Abubakirov, I.R., Droznina, S.Ya., Ivanova, E.I., Matveenko, E.A., Mityushkina, S.V., Ototyuk, D.A., Pavlov, V.M., Raevskaya, A.A., Saltykov, V.A., Senyukov, S.L., Serafimova, Yu.K., Skorkina, A.A., Titkov, N.N., Chebrov, D.V., 2016. The M_w = 7.2, I = 6 (KS = 15.7) Zhupanovskoe earthquake of 30.01.2016 (Kamchatka). Vestnik KRAUNTs, Nauki o Zemle 29 (1), 5–16.

Ershov, I.A., 1974. Seismic risk assessment for Petropavlovsk-Kamchatsky city, in: Seismicity and Seismic Prediction, Upper Mantle Properties and Their Relation with Volcanism in Kamchatka [in Russian]. Nauka, Novosibirsk, pp. 82–90.

Fedotov, S.A., 1972. Energy Classification of Earthquakes in Kuriles-Kamchatka and Problems of Magnitudes [in Russian]. Nauka, Moscow.

Geli, L., Bard, P.Y., Jullien, B., 1988. The effect of topography on earthquake ground motion: a review and new results. Bull. Seismol. Soc. Am. 78 (1), 42–63.

Geophysical Surveys of the Russian Academy of Sciences, Federal Research Center, Kamchatka Branch. A network of strong-motion stations. URL: http:.emsd.ru/133-sd (last visited: 19.11.2018).

Gorbatov, A., Dominguez, J., Suarez, G., Kostoglodov, V., Zhao, D., Gordeev, E., 1999. Tomographic imaging of the *P*-wave velocity

structure beneath the Kamchatka Peninsula. Geophys. J. Int. 137 (2), 269–279.

Gusev, A.A., 1990. Preliminary estimates of seismicity for Petropavlovsk-Kamchatsky. Sources and effects of strong seismic waves. Voprosy Inzhenernoi Seismologii 31, 67–85.

Gusev, A.A., Guseva, E.M., 2014. Scaling properties of corner frequencies of Kamchatka earthquakes. Dokl. Earth Sci. 458 (1), 1112–1115.

Gusev, A.A., Zobin, V.M., Feofilaktov, V.D., 1980. Computed shaking intensity and estimation of strongest earthquake ground motions at a construction site in Kamchatka, in: Quantitative Estimation of Seismic Effects [in Russian]. Nauka, Moscow, p. 44–59.

Gusev, A.A., Skorkina, A.A., Chebrov, D.V., 2017. Spectral source parameters of M_w = 3–6 earthquakes in East Kamchatka, from shear waves. Vestnik KRAUNTS, Nauki o Zemle 35 (3), 36–49.

Hua, Z.-X., Ma, Y.-S., Gao, L.-S., 1993. Site amplification effect of coda waves in West Yunnan Experimental Site. Acta Seismol. Sinica 6 (4), 833–841.

Hudson, D.E., 1972. Local distribution of strong earthquake ground motions. Bull. Seismol. Soc. Amer. 62 (6), 1765–1786.

Jenkins, G.M., Watts, D.G., 1968. Spectral Analysis and Its Applications. Holden-Day, San Francisco, Cambridge, London, Amsterdam.

Joyner, W.B., Fumal, T.E., 1984. Use of measured shear-wave velocity for predicting geologic site effects on strong ground motion, in: Proc. 8th World Conf. Earthquake Engin., Vol. 2, pp. 777–783.

Kotha, S.R., Bindi, D., Cotton, F., 2016. Partially non-ergodic region specific GMPE for Europe and Middle-East. Bull. Earth. Engin. 14 (4), 1245–1263.

Kuzin, I.P., 1974. Focus Zone and Upper Mantle Structure in the Area of East Kamchatka [in Russian]. Nauka, Moscow.

Lemzikov, V.K., Gusev, A.A., 1989. Energy classification of local earthquakes in Kamchatka according to coda amplitudes. J. Volcanol. Seismol. No. 4, 83–97.

Margheriti, L., Wennerberg, L., Boatwright, J., 1994. A comparison of coda and *S*-wave spectral ratios as estimates of site response in the southern San Francisco bay area. Bull. Seismol. Soc. Am. 84 (6), 1815–1830.

Markovskii, B.A. (Ed.), 2000. State Geological Map of the Russian Federation. South Kamchatka Series (N-57-XXXIII: Petropavlovsk-Kamchatsky, N-57-XXXIII: Mutnovskaya Hill). Scale 1:200 000 [in Russian]. Kartfabrika VSEGEI, St. Petersburg.

Medvedev, S.V. (Ed.), 1977. Local-Scale Seismic Risk Zoning [in Russian]. Nauka, Moscow.

Pavlenko, O.V., Irikura, K., 2006. Nonlinear behavior of soils revealed from the records of the 2000 Tottori, Japan, Earthquake at stations of the digital strong-motion network Kik-Net. Bull. Seismol. Soc. Am. 96 (6), 2131–2145.

Petukhin, A.G., Gusev, A.A., 2003. The duration-distance relationship and average envelope shapes of small Kamchatka earthquakes. Pure Appl. Geophys. 160 (9), 1717–1743.

Phillips, W.S., Aki, K., 1986. Site amplification of coda waves from local earthquakes in Central California. Bull. Seismol. Soc. Am. 76 (3), 627–648.

Ratnikova L.I., 1973. Methods for Modeling Seismic Fields in a Thin-Layered Earth [in Russian]. Nauka, Moscow.

Rautian, T.G., Khalturin, V.I.,1978. The use of the coda for determination of the earthquake source spectrum. Bull. Seismol. Soc. Am. 68 (4), 923–948.

Rautian, T.G., Khalturin, V.I., Zakirov, M.S., Zemtsova, A.G., Proskurin, A.P., Pustovitenko, B.G., Pustovitenko, A.N., Sinelnikova, L.G., Filina, A.G., Shengeliya, I.S., 1981. Experimental Studies of Coda Waves [in Russian]. Nauka, Moscow.

Shevchenko, Yu.V., Yakovenko, V.V., 2018. Site correction for energy class and seismic impedance for seismic stations in Kamchatka. J. Volcanol. Seismol. No. 3, 221–230.

Shteinberg, V.V., Fedotov, S.A., 1974. Estimating ground motion in Petropavlovsk-Kamchatsky during possible large earthquakes, in:

Seismicity and Earthquake Prediction, Upper Mantle Properties and Their Relation with Volcanism in Kamchatka [in Russian]. Nauka, Novosibirsk, pp. 90–100.

Sidorenko, A.V., 1964. Geology of the USSR, Book 31. Geological Description. Kamchatka, Kuriles and Commander Islands [in Russian]. Nedra, Moscow.

Sinelnikova, L.G., 1986. Passport of Petropavlovsk-Kamchatsky Seismic Station [in Russian]. Petropavlovsk-Kamchatsky.

Skorkina, A.A., Gusev, A.A., 2017. Determination of corner frequencies of source spectra for subduction earthquakes in Avacha Gulf (Kamchatka). Russian Geology and Geophysics (Geologiya i Geofizika) 58 (7), 844–854 (1057–1068).

Sladnev, B.I., 2007. State Geological Map of the Russian Federation, Scale 1:200 000 (Second edition). Series East Kamchatka. Sheet 0-58-XXVI, XXXI, XXXII (Ust'-Kamchatsk). Explanatory Note [in Russian]. Kartfabrika VSEGEI, St. Petersburg.

Vereshchagin, V.N. (Ed.), 1956. Geological Map of the USSR, Sheet M-56(57). Northern Group of the Kuriles Islands, Scale 1:1 000 000 [in Russian]. Kartfabrika Gosgeoltekhizdat, Moscow.

Zapolsky, K.K., 1971. Frequency-selective seismic stations, in: Experimental Seismology [in Russian]. Nauka, Moscow, pp. 20–36.